Sensitivity of helioseismic gravity modes to the dynamics of the solar core

S. Mathur[1], A. Eff-Darwich[2,3], R.A. García[1], and S. Turck-Chièze[1]

[1] Laboratoire AIM, CEA/DSM – CNRS - Université Paris Diderot – IRFU/SAp, 91191 Gif-sur-Yvette Cedex, France
[2] Departamento de Edafología y Geología, Universidad de La Laguna, Tenerife, Spain
[3] Instituto de Astrofísica de Canarias, 38205, La Laguna, Tenerife, Spain

ABSTRACT

Context. The dynamics of the solar core cannot be properly constrained through the analysis of acoustic oscillation modes. Gravity modes are necessary to understand the structure and dynamics of the deepest layers of the Sun. Through recent progresses on the observation of these modes – both individually and collectively – new information could be available to contribute to inferring the rotation profile down inside the nuclear burning core.
Aims. To see the sensitivity of gravity modes to the rotation of the solar core. We analyze the influence of adding the splitting of one and several g modes to the data sets used in helioseismic numerical inversions. We look for constraints on the uncertainties required in the observations in order to improve the derived core rotation profile.
Methods. We compute forward problems obtaining three artificial sets of splittings derived for three rotation profiles: a rigid profile taken as a reference, a step-like and a smoother profiles with higher rates in the core. We compute inversions based on Regularized Least-Squares methodology (RLS) for both artificial data with real error bars and real data. Several sets of data are used: first we invert only p modes, then we add one and several g modes to which different values of observational uncertainties (75 and 7.5 nHz) are attributed. For the real data, we include g-mode candidate, $\ell=2$, n=-3 with several splittings and associated uncertainties.
Results. We show that the introduction of one g mode in artificial data improves the rate in the solar core and give an idea on the tendency of the rotation profile. The addition of more g modes gives more accuracy to the inversions and stabilize them. The inversion of real data with the g-mode candidate gives a rotation profile that remains unchanged down to 0.2 $R_\odot$, whatever value of splitting we attribute to the g mode.

Key words. Methods: data analysis – Sun: helioseismology, rotation, interior

1. Introduction

The Sun is a magnetic star and it is now well recognized that the dynamical processes occurring in the solar interior are linked to the activity of the visible external layers (For a review of solar and stellar activity see Schrijver & Zwaan (2000)). The fact that the Sun is still active today, even at the present low rotation rate (in comparison to young stars), implies that the initial magnetic fields are maintained, regenerated or amplified through dynamo effects which are induced by fluid motions within the star, namely rotation, convection and/or meridional circulation (support for this comes from observations, e.g., Hartmann & Noyes (1987)). In this sense, it is necessary to reconstruct the solar internal rotational profile from the surface down to the core, to properly understand the magnetic activity of the Sun. Over the past decade, increasingly accurate helioseismic observations from ground-based and space-based instruments have given us a reasonably good description of the dynamics

of the solar interior (Schou et al. 1998; Antia & Basu 2000; Thompson et al. 2003, and references therein). Helioseismic inferences have confirmed that the differential rotation observed at the surface persists throughout the convection zone. There appears to be very little, if any, variation of the rotation rate with latitude in the outer radiative zone (0.4 > $r/R_\odot$ > 0.7). The rotation rate is almost constant (≈ 430 nHz) in this region which is separated from the region of differential rotation by a narrow shear layer —known as the tachocline (Spiegel & Zahn 1992; Corbard et al. 1998) —.

The rotation profile of the Sun is also connected to different aspects of the structure and dynamics of the star. This is the reason why the rotation rate is needed to estimate the circulation and shear instabilities which are responsible for the redistribution of chemical elements (Thompson et al. 2003). Moreover, the redistribution of angular momentum through the coupling between the turbulent convection and the rotation contributes to the strong differential rotation in the convective zone (e.g. Schou et al. 1998) and hence, to the dynamo effect that is

thought to be responsible for the 11-year activity cycle (Brun et al. 2004; Gilman et al. 2007, and references therein) and the evolution of the Hale solar cycle (Dikpati & Gilman 2006).

Although the helioseismic inferences in the radiative zone are not as precise as those found in the convective region, it could be confirmed that the rotation rate is flat and rigid down to approximately 0.4 $R_\odot$. At least three processes have been proposed to explain this flatness of the rotation profile in the radiative zone but without great success: the redistribution of angular momentum by the effect of differential rotation which does not succeed in producing a completely flat profile (Talon & Zahn 1997); the effect of some magnetic fossil field instabilities that could flat the profile but they have not yet been found (Spruit 2002; Eggenberger et al. 2005) and finally, some transport of angular momentum by internal gravity waves (Talon et al. 2002; Charbonnel & Talon 2005; Turck-Chièze & Talon 2007). A general formalism has been developed recently to take into account all these different processes (Mathis & Zahn 2004, 2005), but more accurate observations of the solar rotation profile are needed to constrain the theoretical picture.
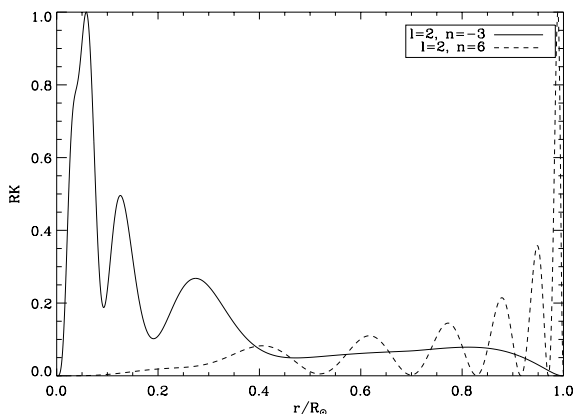

Fig. 1. Rotational kernels for a p mode ($\ell = 2$, n=6) and the g-mode candidate ($\ell = 2$, n=-3).

The analysis of the rotation profile at deeper layers (below 0.4 $R_\odot$) and therefore, inside the solar burning core (where more than half of the solar mass is concentrated) could only be carried out with a few tens of p modes – the low-degree modes ($\ell \leq 3$) –. Indeed, since the dawn of helioseismology when the works by Claverie et al. (1981, 1982) led to the conclusion that the solar core rotates from 2 to 9 times faster than the surface rate, several groups have published different estimations of the rotation rate in the solar core – using acoustic modes – with contradictory results (Jimenez et al. 1994; Elsworth et al. 1995; Fossat et al. 1995; Lazrek et al. 1996; Chaplin et al. 2001). The importance of the low order p modes (below 2.3 mHz) to properly establish the profile below 0.4 $R_\odot$ has been shown (Couvidat et al. 2003). Gravity modes having large sensitivities to the solar core, will significantly contribute to establish

the actual dynamical conditions of the core. This is illustrated in Fig. 1 representing the rotational kernel for a g mode ($\ell = 2$, $n = -3$) and for a p mode ($\ell = 2$, $n = 6$). This g mode is mostly sensitive to the region below 0.2 $R_\odot$ whereas the p mode is sensitive to the region above 0.4 $R_\odot$. It shows the importance of g modes compared to p modes for having access to the rotation of the core.

The advent of the new millennium saw the burgeoning of the g-mode research based on the quality and accumulation of helioseismic data. In 2000, Appourchaux et al. looked for individual spikes above 150 μHz in the power spectrum with more than 90% confidence level that the signal was not pure noise. Although they could not identify any g-mode signature, an upper limit of their amplitudes could be established: at 200 μHz, they would fall below 10 mms^{-1} in velocity, and below 0.5 parts per million in intensity. Later, in 2002, Gabriel et al., using the same statistical approach, found a peak that could be interpreted as one component of the ℓ=1, n=1 mixed mode.

A different approach based on the search of multiplets and recurrent signals in time (García & Turck-Chièze 1997; Pallé & García 1997; Turck-Chièze et al. 1998) have been applied to GOLF[1]/SoHO[2] velocity time series (García et al. 2005). Some time-coherent patterns were found in the signal (Gabriel et al. 1999), thus they could be potentially considered as g modes. Turck-Chièze et al. (2004) applied this technique to high-frequency multiplets in hope of reducing the detection threshold while maintaining the same confidence level. These authors found several patterns attributed to g-mode signals and, in particular, one was considered as a candidate for the mode $\ell = 2, n = -3$. In fact, Cox & Guzik (2004) postulated theoretically that this mode could be the one with the largest amplitude at the solar surface. This candidate is still present in the analysis of longer time series (Mathur et al. 2007, and references therein). Finally, the measurement of a signal that could be attributed to the separation in period of the dipole gravity modes and the comparison with solar models fosters a faster rotation rate in the core than the rest of the radiative zone (García et al. 2007).

In this work, we will study how the inferences about the solar core rotation profile could be improved by including gravity modes. We will study the effect of adding either one (the candidate ℓ=2 n=-3) or several g modes in the data set that will be inverted to infer the rotational profile. The effect of the observational uncertainties on the derived rotational rate will also be analyzed, as well as the introduction of the g-mode candidate in real p-mode data sets.

2. Methodology.

Helioseismic inferences on the internal rotation rate of the Sun are carried out through numerical inversions of the functional form of the perturbation in frequency, $\Delta \nu_{n\ell m}$, induced by the ro-

---

[1] Global Oscillations at Low Frequency (Gabriel et al. 1995)

[2] Solar and Heliospheric Observatory (Domingo et al. 1995)

tation of the Sun, $\Omega(r, \theta)$ and given by (see derivation in Hansen et al. 1977):

$$\Delta\nu_{n\ell m} = \frac{1}{2\pi} \int_0^R \int_0^\pi K_{n\ell m}(r, \theta)\Omega(r, \theta)drd\theta + \epsilon_{n\ell m} \qquad (1)$$

The perturbation in frequency, $\Delta\nu_{n\ell m}$ with error $\epsilon_{n\ell m}$, that corresponds to the rotational component of the frequency splittings, is given by the integral of the product of a sensitivity function, or kernel, $K_{n\ell m}(r, \theta)$ with the rotation rate, $\Omega(r, \theta)$, over the radius, r, and the co-latitude, θ. The kernels, $K_{n\ell m}(r, \theta)$, are known functions of solar models.

Equation 1 defines the forward problem for the solar interior rotation rate through global helioseismology, since it is possible to calculate estimates of the frequency splittings, $\Delta\nu_{n\ell m}$, that correspond to a given solar rotation rate, $\Omega(r, \theta)$.
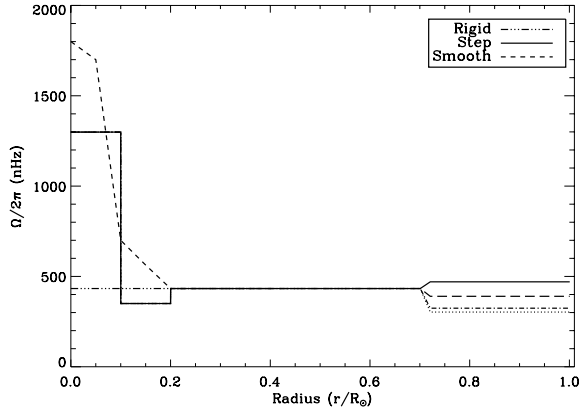

Fig. 2. Artificial rotation profiles for the solar interior as explained in the text and used in the computation of the artificial data sets. The three artificial profiles have the same behavior in the convective zone. They incorporate latitudinal variations in the convection zone to mimic the actual rotation profile of the Sun. The plotted latitudes are 0° (solid line), 30° (dashed line), 60° (dotted line) and 75° (dashed-dotted line).

The latter equation also defines a classical inverse problem for the sun's rotation. The inversion of this set of M integral equations – one for each measured $\Delta\nu_{n\ell m}$ – allows us to infer the rotation rate profile as a function of radius and latitude from a set of observed rotational frequency splittings (hereafter referred to as splittings). The inversion method we have used is based on the regularized least-squares methodology (RLS). The RLS method requires the discretization of the integral relation to be inverted. In our case, Eq. 1 is transformed into a matrix relation

$$D = Ax + \epsilon \qquad (2)$$

where D is the data vector, with elements $\Delta\nu_{n\ell m}$ and dimension M, x is the solution vector to be determined at N tabular points,

A is the matrix with the kernels, of dimension $M \times N$ and ϵ is the vector containing the errors in D.

The RLS solution is the one that minimizes the quadratic difference $\chi^2 = |Ax - D|^2$, with a constraint given by a smoothing matrix, H, introduced in order to lift the singular nature of the problem (see, for instance, Eff-Darwich & Pérez Hernández 1997). Hence, the function x is approximated by

$$x_{\text{est}} = (A^T A + \Lambda H)^{-1} A^T D \qquad (3)$$

where Λ is a vector defining how much regularization is applied to each point x_i of the inversion mesh, as introduced in Eff-Darwich & Pérez Hernández (1997).

As a by-product of the inversion methodology, we could replace D from Eq. 2 to obtain

$$x_{\text{est}} = (A^T A + \Lambda H)^{-1} A^T Ax \overset{\text{def}}{=} Rx \qquad (4)$$

hence

$$R = (A^T A + \Lambda H)^{-1} A^T A \qquad (5)$$

The matrix R, that combines forward and inverse mapping, is referred to as the resolution or sensitivity matrix, while the i_{th} row is referred as the resolution kernel for the estimation of x_i (Eff-Darwich et al. 2008). The diagonal elements R_{ii} state how much of the information is saved in the model estimate and may be interpreted as the resolvability or sensitivity of x_i. In this sense, it could be possible to use R_{ii} to see the effect of modifying the mode sets used in the inversion on the resolvability of each point of the inversion mesh.
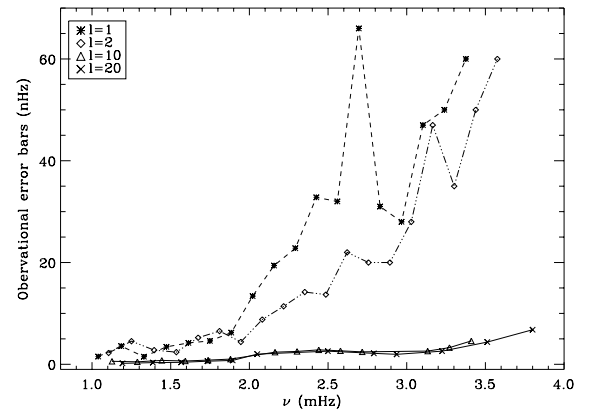

Fig. 3. Observational error bars of p-mode splittings for degrees $\ell=1, 2$, 10 and 20 as a function of the central frequency of the mode. Each degree is represented by a symbol as explained in the legend of the figure.

A theoretical analysis was carried out in order to determine the effect of the addition of g modes on the derivations of the solar rotation rate of the burning core. Different artificial data

sets have been calculated using Eq. 1 and three artificial rotation rates $\Omega(r, \theta)$ that are shown in Fig.2. They all have a differential rotation in the convection zone and a rigid rotation from 0.7 down to 0.2 $R_\odot$ equal to Ω_{rz}=433 nHz. In the first profile – the rigid profile –, that is our reference profile, the flat and rigid rotation includes the core. The second profile – the step profile –, is a step-like profile having a rate 3 times larger than the rest of the radiative zone below 0.1 $R_\odot$ and a rate of 350 nHz in the region 0.1-0.2 $R_\odot$. Though this profile has unrealistic steep changes, it is useful to check the quality of the inversion as these steep profiles are difficult to reproduce. The rotational rate for the third profile – the smooth profile – increases gradually from 433 nHz at 0.2 $R_\odot$ reaching 1800 nHz in the centre, being in this sense compatible with the latest theoretical studies.
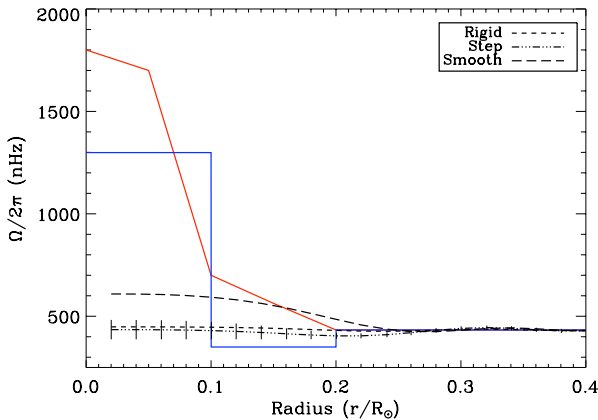

Fig. 4. Equatorial rotation profiles below 0.4 $R_\odot$ reconstructed with the p modes (Set D_1) for the rigid profile (dotted line), the step profile (triple dotted-dashed line) and the smooth profile (dashed line). For the sake of clarity we have plotted the error bars in the step profile only. The continuous blue, red and small dashed lines are respectively the step, smooth and rigid artificial rotation profiles.

The different artificial data sets correspond to different mode sets, as explained in Table 1. The observational uncertainties for p modes (see Fig. 3) were calculated through Principal Component Analysis of the mode sets extracted from a sample of 728 days-long MDI[3] time-series (Korzennik 2005) for p modes with degrees ranging from ℓ=4 to 25, whereas for ℓ=1, 3 modes, the uncertainties were extracted from a combined GOLF-MDI time series (García et al. 2004). The degree range of all data sets spans from ℓ=1 to 25, however the frequency range of the artificial data sets depends on the degree of the mode, ranging from 1 to 2.3 mHz for ℓ=1 to 3 and from 1 to 3.9 mHz for ℓ=4 to 25. As it is illustrated in Fig. 3, the uncertainties above 2.3 mHz for low degree modes are very large,

___

[3] Michelson Doppler Imager (Scherrer et al. 1995)

since it is more difficult to estimate the splittings as a consequence of the blending between the multiplet components of the modes due to the reduction in their life times (Bertello et al. 2000; García et al. 2001, 2004; Chaplin et al. 2002; Couvidat et al. 2003). Up to eight different g modes have been used in this work, four ℓ=1 (with frequencies down to 100 μHz) and four ℓ=2 (with frequencies down to 150 μHz) which are the modes with the highest predicted amplitudes (Kumar et al. 1996; Provost et al. 2000). Since g modes have not yet been characterized, different theoretical uncertainties have been used during the inversion process. Indeed the first value of 75 nHz for the uncertainty on the g-mode splitting, corresponds to the tolerance in the search algorithm used by Turck-Chièze et al. (2004) and is related to a possible shift of the multiplet components due to the presence of a central magnetic field. Rashba et al. (2007) have already shown that this would shift the central frequencies of g modes in this region by such amount. The other value of 7.5 nHz is a typical uncertainty that could be obtained by fitting dipolar modes with ~ 4 years of data and could be a good example of what we could measure in the near future with the next generation of instruments.

3. Results

3.1. Inversions of artificial data

A set of numerical inversions were carried out to study the effect of adding g modes on the derivation of the rotation rate of the solar core. The analysis of the inversion results were complemented with the study of the resolution kernels of the inversions and the direct comparison of the sets of frequency splitting used.
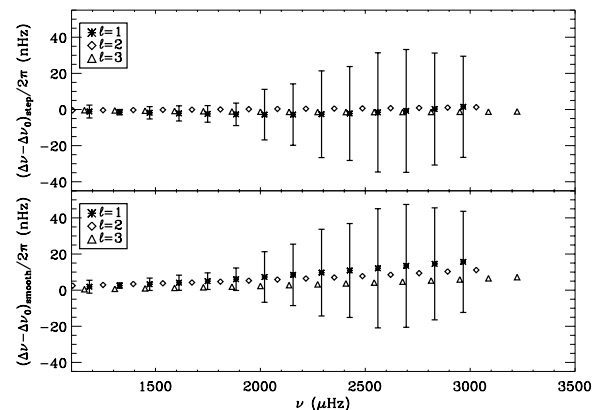

Fig. 5. Difference of the p-mode splittings between the step profile and on the one hand the rigid profile (top) and on the other hand, the smooth profile (bottom).
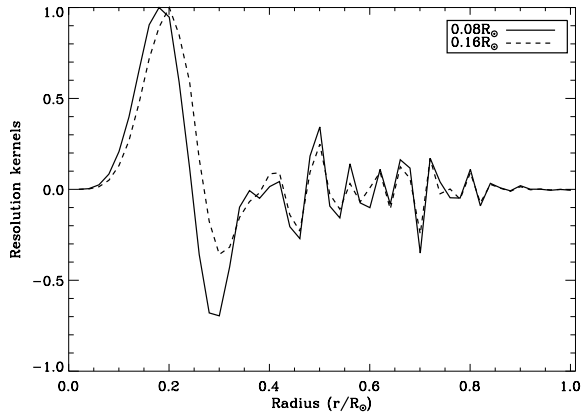
The inversion of the available p-mode splittings (see Fig.4), as those included in set D_1, reveals that it is not possible to re-

Table 1. Description of the artificial data sets used to study the sensitivity of p and g modes to the dynamics of the solar core.
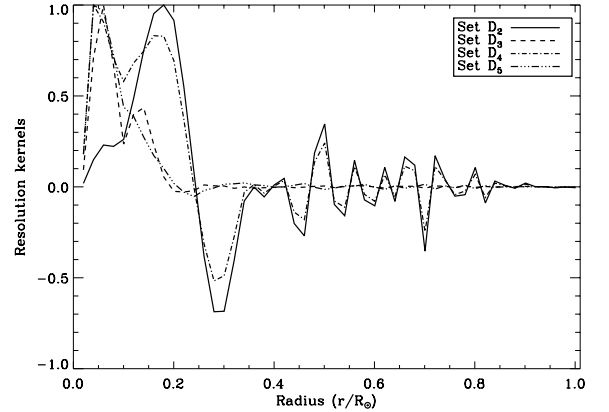
| Data set | Freq. range (mHz) | | | |
	g modes	Uncertainty on g modes (nHz)	p modes $\ell = 1, 3$	p modes $\ell > 3$
Set D_1	-	-	$1 \leq \nu \leq 2.3$	$1 \leq \nu \leq 3.9$
Set D_2	$\ell = 2, n = -3$	75	$1 \leq \nu \leq 2.3$	$1 \leq \nu \leq 3.9$
Set D_3	$\ell = 2, n = -3$	7.5	$1 \leq \nu \leq 2.3$	$1 \leq \nu \leq 3.9$
Set D_4	$\ell = 1, n = -2$ to -5 and $\ell = 2, n = -3$ to -6	75	$1 \leq \nu \leq 2.3$	$1 \leq \nu \leq 3.9$
Set D_5	$\ell = 1, n = -2$ to -5 and $\ell = 2, n = -3$ to -6	7.5	$1 \leq \nu \leq 2.3$	$1 \leq \nu \leq 3.9$

cover any of the three artificial rotation profiles below 0.2 $R_\odot$ (see Fig.2). This result is also illustrated by the comparison of the splittings calculated from the rigid, step and smooth profiles (see Fig.5), since such differences fall below 1 nHz, being the present level of uncertainties for these splittings above this value. The resolution kernels for these inversions (Fig.6) also confirm the lack of sensitivity below 0.2 $R_\odot$, since it is not possible to properly locate and recover the resolution kernels below 0.2 $R_\odot$.

the g mode (with an error bar of 75 nHz), when compared to the same resolution kernel calculated from the inversion of p modes. Unlike the splittings calculated for p modes, the differences in the frequency splittings calculated from the three artificial rotational profiles for the g modes could be larger than 200 nHz (see Fig.10). It is shown in this figure that the differences of splittings calculated for a rigid profile and for the other two simulated rotation profiles, are around 200 nHz. This means that following the usual criteria of ~3 σ to have a proper detection, a difference of 200 nHz is visible with the modes having an uncertainty of 75 nHz. Therefore, in this condition, it is possible to discriminate between the rigid profile and the other one with a higher rotation rate in the core.

Fig. 6. Resolution kernels computed in the inversion of the set D_1 containing only p modes and calculated at two radii: 0.08 $R_\odot$ (solid line) and 0.16 $R_\odot$ (dashed line).

Fig. 7. Resolution kernels computed in the inversion of the set D_2 (i.e. including the g mode $\ell=2$ $n=-3$ with an error bar of 75 nHz), D_3(i.e., including the g mode with an error bar of 7.5 nHz), D_4 (i.e., including eight g modes with an error bar of 75 nHz) and D_5 (i.e., including eight g modes with an error bar of 7.5 nHz) at 0.08 $R_\odot$.

When one g mode ($\ell=2$, n=-3 around 220 μHz) is added to the p-mode data set, as in the case of sets D_2 and D_3, the inversion results improve below 0.1 $R_\odot$ (see Fig.8 and Fig.9), but there is not substantial improvement around 0.2 $R_\odot$. The match between the artificial rotational profiles and the profiles estimated from the inversions improves when the error assigned to the g mode is reduced. Unlike the case of the inversion of only p modes, the resolution kernels at 0.08 $R_\odot$ significantly improves when adding one g mode (see Fig.7), in particular when the observational uncertainty falls to 7.5 nHz. The resolution kernel at 0.16 $R_\odot$ does not change (or slightly) with the addition of

If eight g modes are added to the p-mode data set, as in sets D_4 and D_5, the inversion results (see Figs.8 and 9) in both the level of uncertainties of the estimates and the matching to the proxy rotation profiles are significantly better than those
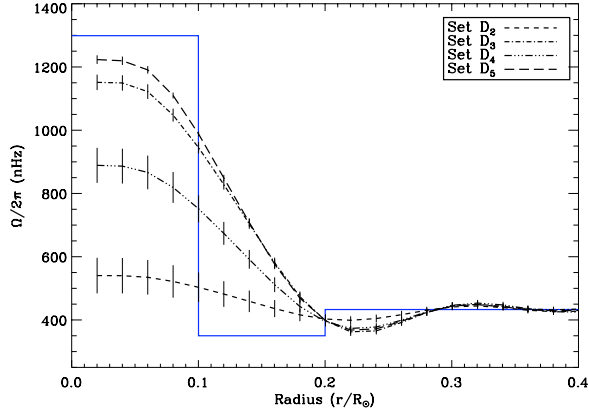
Fig. 8. Equatorial rotation profiles below 0.4 $R_\odot$ reconstructed from the set D_2 (i.e., including the g mode $\ell=2$ $n=-3$ with an error bar of 75 nHz), D_3(i.e., including the g mode with an error bar of 7.5 nHz), D_4 (i.e., including eight g modes with an error bar of 75 nHz) and D_5 (i.e., including eight g modes with an error bar of 7.5 nHz) for the step profile.
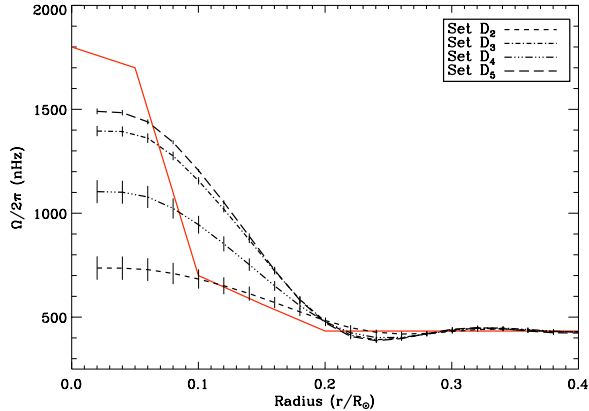

Fig. 9. Equatorial rotation profiles below 0.4 $R_\odot$ reconstructed from the set D_2 (i.e., including the g mode $\ell=2$ $n=-3$ with an error bar of 75 nHz), D_3(i.e., including the g mode with an error bar of 7.5 nHz), D_4 (i.e., including eight g modes with an error bar of 75 nHz) and D_5 (i.e., including eight g modes with an error bar of 7.5 nHz) for the smooth profile. Same legend as Fig.8.

obtained from the inversion with only one g mode. The differences in the frequency splittings calculated from the three artificial rotational profiles for all the eight g modes are significantly larger than the observational uncertainties and hence, new information could be gained as compared to that given by just one g mode. This is particularly important in the presence

of noisy data, since the larger the number of g modes, the better the averaging of the unwanted effects of the noise in the data will be. The addition of several g modes helps to better define the resolution kernels below 0.1 $R_\odot$ (see the resolution kernel at 0.08 $R_\odot$ Fig. 7), whereas the resolution kernel at 0.16 $R_\odot$ does not significantly change by the addition of g modes. In this sense, the inferences about the rotational rate of the core will be significantly improved below 0.1 $R_\odot$, where the energy of the g modes is maximum. Very high frequency p modes (above 2.5 mHz) for $\ell=1$ and 2 should be characterized to better define the region between 0.15 and 0.25 $R_\odot$ (Garcia et al. 2008)
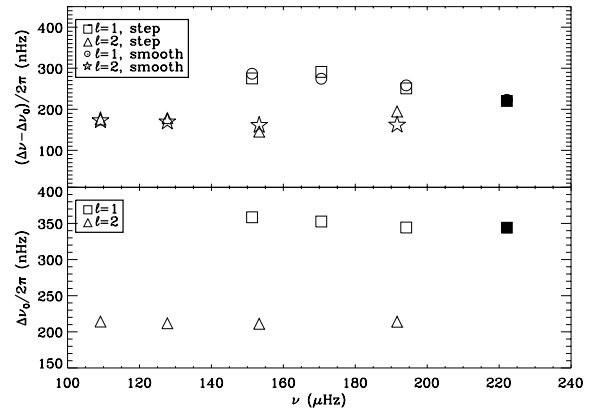

Fig. 10. Splittings differences of g modes between the rigid profile and on one hand, the step profile and on the other hand, the smooth profile (top). We have only represented the eight g modes used in the inversions. The filled square corresponds to the g-mode candidate $\ell=2$ n=-3. We have also plotted the splittings of these modes for the rigid profile (bottom).

3.2. Inversion of real data

We have used inversions to study the compatibility of present p-mode frequency splittings with the splittings estimated by Turck-Chièze et al. (2004) for the $\ell=2$, n=-3 g mode. The p-mode set corresponds to the mode set used in D_1, where the splittings correspond to those calculated by Korzennik (2005) for 2088 day-long MDI time-series. In Turck-Chièze et al. (2004), three scenarios were proposed to explain the detected pattern around 220 μHz, with two possible values for the splittings, namely 300 nHz, if this were a detection of two modes (a combination of an $\ell=2$ and a $\ell=5$), and 600 nHz, if all the visible components correspond to the same mode (the $\ell=2$ n=-3 which implies an inclined core rotation axis).

Five inversions are carried out (see Fig.11), namely one inversion including only p modes and other four containing one g mode, but with different estimates of the frequency splitting (300 and 600 nHz) and two observational uncertainties (75 and 7.5 nHz). As it was illustrated in Figs. 4, 5 and 6, there is no

sensitivity of the observed p modes to the dynamics of the inner solar core. Different rotational profiles below 0.2 $R_\odot$ are obtained for the different combinations of the value of the introduced g-mode splitting and its corresponding uncertainty. In all cases, these values are compatible with the data calculated for the p modes in the sense that the inversions are unchanged and stable (e.g. the inversion does not show any oscillatory behaviour) above 0.2 $R_\odot$ when the g mode is added to the data set. In Fig.8, an oscillation around 0.2 $R_\odot$ appears with the artificial data when g modes are associated to an error bar of 7.5 nHz. This is also observed with the real data. This is an artefact of the inversion. The rotation profile obtained using the highest value of the g-mode splitting (600 ±7.5 nHz) proposed by Turck-Chièze et al. (2004), gives a rate in the inner core that is compatible with the result from the dipole analysis carried out by García et al. (2007).

To quantify the compatibility between the p-mode data and the g-mode candidate, we have calculated the normalised residuals for all the observed modes (ℓ, m, n) defined by $(\delta\nu_{\text{data}} - \delta\nu_{\text{inv}})/\sigma$, where $\delta\nu_{\text{data}}$ is the value of the splitting in the data, $\delta\nu_{\text{inv}}$, the value corresponding to the rotation profile obtained with the inversion and σ, the error bar associated to the splitting of the mode. Table 2 gives the mean value of these residuals for the low-degree p modes ($\ell \leq 3$, below 2 mHz) and the g-mode candidate for the four inversions (the two values for the splittings and the two values for the uncertainty for the g mode). We can see that the difference of splitting between the real data and the results of the forward problem on the inferred rotation profile is less than 1.5 σ for the p modes. However, for the g-mode candidate, this difference goes up to ~3 σ. This is due to the fact that the rotation profile has some uncertainties that have an impact on the splittings calculated. Globally, the results with the g-mode candidate are compatible with the information contained in the observed p-mode data.
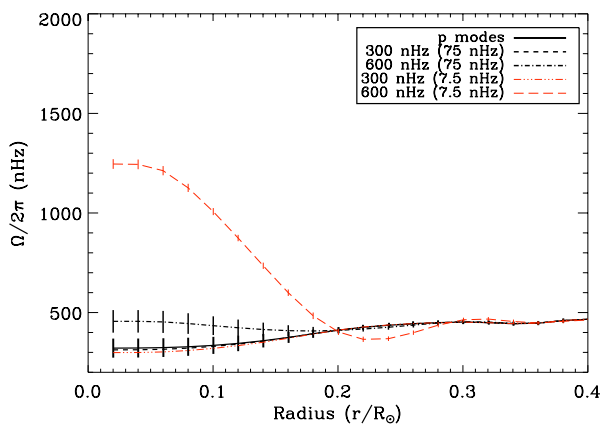
4. Conclusions

In this paper, we have studied how the inversion of several artificial rotation profiles could be improved when g modes are added to the present set of observed p modes. The introduction of one g mode –the candidate $\ell=2$, n=-3– significantly improves the solution in the inner core (below 0.1 $R_\odot$), when compared to that obtained using only p modes. It gives the general trend of the solar core rotation but there is not accurate information on the profile itself. If more g modes are added to the inversion data set (four $\ell=1$ and four sectoral $\ell=2$), the result in terms of accuracy and error propagation, improves compared with the inversion including only 1 g mode. However there is still information missing in the region between 0.1 - 0.2 $R_\odot$, where the energy of the g modes is significantly lower than in the region below 0.1 $R_\odot$. The information given by the p modes is negligible due to the lack of sensitivity to these depths, the high level of uncertainties we have in their determination and the noise present in the data.

Finally, for the real data, the rotation profile obtained using the highest value of the g-mode splitting gives a rate in the inner core that is compatible with the result obtained with an independent technique by García et al. (2007), if we put an error bar of 7.5 nHz. Moreover, we obtained a limit down to which we can trust the inversion of the real data. All the values proposed for the splittings of the $\ell=2$, n=-3 g-mode candidate are compatible with the splittings calculated for the p modes. Indeed, having in mind that the small oscillation is related to the inversion and not to the data, the addition of the g-mode candidate with different values for the splitting and their uncertainty, does not change the estimated profile above 0.2 $R_\odot$.

References

Antia, H. M. & Basu, S. 2000, ApJ, 541, 442

Appourchaux, T., Fröhlich, C., Andersen, B., et al. 2000, ApJ, 538, 401

Bertello, L., Varadi, F., Ulrich, R. K., et al. 2000, ApJ, 537, L143

Brun, A. S., Miesch, M. S., & Toomre, J. 2004, ApJ, 614, 1073

Chaplin, W. J., Elsworth, Y., Isaak, G. R., et al. 2001, MNRAS, 327, 1127

Chaplin, W. J., Elsworth, Y., Isaak, G. R., et al. 2002, MNRAS, 336, 979

Charbonnel, C. & Talon, S. 2005, Science, 309, 2189

Claverie, A., Isaak, G. R., McLeod, C. P., et al. 1982, Nature, 299, 704

Claverie, A., Isaak, G. R., McLeod, C. P., van der Raay, H. B., & Roca Cortes, T. 1981, Nature, 293, 443

Corbard, T., Berthomieu, G., Provost, J., & Morel, P. 1998, A&A, 330, 1149

Fig. 11. Equatorial rotation profiles reconstructed with the real data as explained in the text and adding the g-mode candidate $\ell=2$ n=-3 with two different splittings (300 and 600 nHz) combined with two different error bars (75 and 7.5 nHz).

---

[4] http://www.helas-eu.org/

Table 2. Normalised residuals for p modes (ℓ =1, 2 and 3 and $\nu \leq 2$ mHz) and the g-mode candidate.

	600 nHz, $\epsilon = 75$ nHz	600, nHz $\epsilon = 7.5$ nHz	300 nHz, $\epsilon = 75$ nHz	300 nHz, $\epsilon = 7.5$ nHz
$\ell = 1$	-0.13	- 0.69	-0.03	-0.02
$\ell = 2$	0.34	-0.42	0.47	0.49
$\ell = 3$	-1.13	-1.23	-1.10	-1.10
$\ell = 2, n = -3$	3.36	2.16	-0.05	-0.04

Couvidat, S., García, R. A., Turck-Chièze, S., et al. 2003, ApJ, 597, L77

Cox, A. N. & Guzik, J. A. 2004, ApJ, 613, L169

Dikpati, M. & Gilman, P. A. 2006, ApJ, 649, 498

Domingo, V., Fleck, B., & Poland, A. I. 1995, Sol. Phys., 162, 1

Eff-Darwich, A., Korzennik, S. G., Jiménez-Reyes, S. J., & García, R. A. 2008, ApJ, Accepted (http://arXiv.org/abs/0802.3604)

Eff-Darwich, A. & Pérez Hernández, F. 1997, A&AS, 125, 391

Eggenberger, P., Maeder, A., & Meynet, G. 2005, A&A, 440, L9

Elsworth, Y., Howe, R., Isaak, G. R., et al. 1995, Nature, 376, 669

Fossat, E., Loudagh, S., Gelly, B., et al. 1995, in Astronomical Society of the Pacific Conference Series, Vol. 76, GONG 1994. Helio- and Astro-Seismology from the Earth and Space, ed. R. K. Ulrich, E. J. Rhodes, Jr., & W. Dappen, 24–+

Gabriel, A. H., Baudin, F., Boumier, P., et al. 2002, A&A, 390, 1119

Gabriel, A. H., Grec, G., Charra, J., et al. 1995, Sol. Phys., 162, 61

Gabriel, A. H., Turck-Chièze, S., García, R. A., et al. 1999, Advances in Space Research, 24, 147

García, R. A., Corbard, T., Chaplin, W. J., et al. 2004, Sol. Phys., 220, 269

Garcia, R. A., Mathur, S., Ballot, J., et al. 2008, Sol. Phys., Accepted (http://arxiv.org/abs/0802.1510)

García, R. A., Régulo, C., Turck-Chièze, S., et al. 2001, Sol. Phys., 200, 361

García, R. A. & Turck-Chièze, S. 1997, Proceedings of the 1997 GOLF annual meeting, Orsay, France

García, R. A., Turck-Chièze, S., Boumier, P., et al. 2005, A&A, 442, 385

García, R. A., Turck-Chièze, S., Jiménez-Reyes, S. J., et al. 2007, Science, 316, 1591

Gilman, P. A., Dikpati, M., & Miesch, M. S. 2007, ApJS, 170, 203

Hansen, C. J., Cox, J. P., & van Horn, H. M. 1977, ApJ, 217, 151

Hartmann, L. W. & Noyes, R. W. 1987, ARA&A, 25, 271

Jimenez, A., Perez Hernandez, F., Claret, A., et al. 1994, ApJ, 435, 874

Korzennik, S. G. 2005, ApJ, 626, 585

Kumar, P., Quataert, E. J., & Bahcall, J. N. 1996, ApJ, 458, L83+

Lazrek, M., Pantel, A., Fossat, E., et al. 1996, Sol. Phys., 166, 1

Mathis, S. & Zahn, J.-P. 2004, A&A, 425, 229

Mathis, S. & Zahn, J.-P. 2005, A&A, 440, 653

Mathur, S., Turck-Chièze, S., Couvidat, S., & García, R. A. 2007, ApJ, 668, 594

Pallé, P. L. & García, R. A. 1997, Proceedings of the 1997 GOLF annual meeting, Orsay, France

Provost, J., Berthomieu, G., & Morel, P. 2000, A&A, 353, 775

Rashba, T. I., Semikoz, V. B., Turck-Chièze, S., & Valle, J. W. F. 2007, MNRAS, 377, 453

Scherrer, P. H., Bogart, R. S., Bush, R. I., et al. 1995, Sol. Phys., 162, 129

Schou, J., Antia, H. M., Basu, S., et al. 1998, ApJ, 505, 390

Schrijver, C. J. & Zwaan, C. 2000, Solar and Stellar Magnetic Activity (Solar and stellar magnetic activity / Carolus J. Schrijver, Cornelius Zwaan. New York : Cambridge University Press, 2000. (Cambridge astrophysics series ; 34))

Spiegel, E. A. & Zahn, J.-P. 1992, A&A, 265, 106

Spruit, H. C. 2002, A&A, 381, 923

Talon, S., Kumar, P., & Zahn, J.-P. 2002, ApJ, 574, L175

Talon, S. & Zahn, J.-P. 1997, A&A, 317, 749

Thompson, M. J., Christensen-Dalsgaard, J., Miesch, M. S., & Toomre, J. 2003, ARA&A, 41, 599

Turck-Chièze, S., Brun, A. S., & Garcia, R. A. 1998, in ESA Special Publication, Vol. 418, Structure and Dynamics of the Interior of the Sun and Sun-like Stars, ed. S. Korzennik, 549–+

Turck-Chièze, S., García, R. A., Couvidat, S., et al. 2004, ApJ, 604, 455

Turck-Chièze, S. & Talon, S. 2007, Advances in Space Research, Available online